Theor Chem Acc (2011) 129:467–481
DOI 10.1007/s00214-010-0885-5

REGULAR ARTICLE

Geometries, electronic structures, and excited states of UN_2, NUO^+, and UO_2^{2+}: a combined CCSD(T), RAS/CASPT2 and TDDFT study

Fan Wei · Guoshi Wu · W. H. Eugen Schwarz · Jun Li

Received: 14 November 2010 / Accepted: 30 December 2010 / Published online: 26 January 2011
© Springer-Verlag 2011

Abstract The ground- and excited-state geometries and electronic structures of the isoelectronic series of molecules UN_2, NUO^+, and UO_2^{2+} are investigated by using relativistic density functional theory (DFT) and ab initio wavefunction theory (WFT). Scalar relativistic and spin–orbit-coupled quantum chemical methods at the CASPT2, RASPT2, CCSD(T), DFT and TDDFT levels are applied. Relativistic effects as elucidated by Pekka Pyykkö play an important role in these uranium compounds, in particular for the excited states. The three molecular species exhibit significantly different spectroscopic properties, concerning their excitation energies, bond lengths and vibrations. Density functional approaches yield qualitatively correct results for the ground states and the valence → U.7s,6d excited states. However, the performance of TDDFT for valence → U.5f type excitations (in particular of UN_2 and NUO^+) is less satisfactory, indicating the importance of the self-interaction correction for such excitations.

Dedicated to Professor Pekka Pyykkö on the occasion of his 70th birthday and published as part of the Pyykkö Festschrift Issue.

Electronic supplementary material The online version of this article (doi:10.1007/s00214-010-0885-5) contains supplementary material, which is available to authorized users.

F. Wei · G. Wu · W. H. E. Schwarz · J. Li (✉)
Theoretical and Computational Chemistry Laboratory, Department of Chemistry, Tsinghua University, 100084 Beijing, China
e-mail: junli@tsinghua.edu.cn

W. H. E. Schwarz
Physical Chemistry, University of Siegen, 57068 Siegen, Germany
e-mail: schwarz@chemi.uni-siegen.de

Keywords Uranium · UN_2 · UNO^+ · UO_2^{2+} · Uranyl · Excited states · Electron correlation · Relativistic effects · Density functional theory

1 Introduction

1.1 The isoelectronic relatives of uranyl

As a ubiquitous moiety, the uranyl dication $[OUO]^{2+}$ is known as the most common building block in uranium chemistry. Experimental investigations of isolated uranyl is challenging because of the difficulty in forming this dication in gas phase [1–3]. The isoelectronic counterparts NUN and $[NUO]^+$ have been formed experimentally as free species [4] or in low-temperature noble-gas matrices [5–9]. Moreover, solid UN_2 is a possible intermediate of the synthesis of uranium mononitride, a potential fuel for next-generation nuclear power systems [10]. The investigation of multiple-bonded uranium main-group compounds has become of topical chemical interest [11–14].

A first and comprehensive theoretical study of the whole group of UO_2^{2+} isoelectronics in their ground states had been undertaken by Pyykkö et al. [15]. Later, Kaltsoyannis [16], Gagliardi et al. [17], and Bursten et al. [18] had calculated uranium triatomic species including NUN, NUO^+, and UO_2^{2+} using DFT and ab initio methods. Subsequently, the heat of formation and the low-lying excited states and spectra of UO_2^{2+} were investigated in more detail by several groups [19–25]. The electronic structures of uranyl and its analogues were reviewed by Pepper and Bursten [26] and Denning [27]. Here, we investigate the similarities and some unexpected differences in the ground and excited states and spectra of molecular NUN, NUO^+, and UO_2^{2+}.

1.2 Methodologies

It is known from Pekka Pyykkö's works, e.g. [15, 28–30], that the properties of uranium compounds are strongly influenced by relativistic modifications of the U.6p semicore and U.5f,6d,7s valence shells. The performance of relativistic effective core potentials (RECP) and of various theoretical methods for these species was assessed by Odoh and Schreckenbach [31]. While scalar relativistic (SR) approaches may be sufficient for the closed-shell ground states, spin–orbit (SO) relativistic methods are necessary for the excited states. All electron (AE) calculations (with or without frozen atomic cores) using the relativistic zero-order regular approximation (ZORA) and RECP calculations were performed on the title molecules. The large number and complex structure of the actinide valence shells consisting of compact 5f, intermediate 6d and more extended 7s atomic orbitals (AOs), and the softness of the outer 6p core shell require sophisticated methods for treating static and dynamic electron correlation and SO-induced splitting.

The above-mentioned theoretical works applied correlation methods up to CCSD(T) (coupled cluster with singles, doubles and triples) and RASPT2 (restricted active space with 2nd order perturbation theory) or CASPT2[g_1] (complete active space with 2nd order perturbation theory), where g_1 corrects for open versus closed-shell differences. For the low-lying excited states of UO_2^{2+}, Pierloot [20, 21] had suggested to keep the U.6p and O.2s semicore shells closed, and to include in the active space only 12 of the 16 valence electrons, and 14–18 orbitals, namely the upper 6 occupied bonding orbitals and an aptly chosen set of non-bonding and antibonding ones. With such a choice of the active space, most of the variation of static and dynamic correlation effects seems to have been recovered thereby.

We will here apply a similar strategy to the titled molecules, although it becomes rather demanding when potential energy surfaces of many excited states are to be determined. Inasmuch as the computational cost of CASSCF increases rapidly upon enlarging the number of active electrons or the space of active orbitals, we will also investigate the efficiency of the RASSCF scheme [32]. In addition, we will evaluate the reliability of popular DFT, SO-DFT, and SO-TDDFT approaches for these actinide compounds.

The applied multi-configuration (MC) and DFT computational procedures are described in Sect. 2. The results of the explicitly correlated ab initio methods are presented and discussed in Sect. 3, while the DFT results are analyzed in Sect. 4. Our conclusions are summarized in Sect. 5.

2 Computational methods

The ab initio calculations were performed using the MOLPRO 2008 program [33] (see SI file). A quasi-relativistic effective-core SO-pseudopotential (RECP) Hamiltonian was used with a uranium 60-electron "U.1s-4f small core" [34], i.e. a total of 32 electrons were treated explicitly. We used the RECP-adapted [12s11p10d8f]/[8s7p6d4f] SDD valence basis set for uranium [34] and the [10s5p2d]/[4s3p2d] aug-cc-pVDZ basis sets [35] for nitrogen and oxygen, all of contracted Gaussian type.

For the SO-averaged SR-CASSCF-based calculations, we included 12 valence electrons from the upper bonding orbitals ($2\sigma_g$, $2\sigma_u$, $1\pi_g$, $1\pi_u$, see Fig. 1); a variety of active spaces with up to 16 orbitals were considered. Calculations with larger active space than these become rather time consuming for the CASPT2 and RASPT2 calculations of the potential energy surfaces. The chosen active spaces consist of the aforementioned 6 upper occupied bonding orbitals ($2\sigma_g$, $2\sigma_u$, $1\pi_g$, $1\pi_u$), of their 6 anti-bonding counterparts (U.7s-$3\sigma_g$*, $3\sigma_u$*, $2\pi_g$*, $2\pi_u$*) and of 2 or 4 from the six intermediate non-bonding orbitals (U.5fϕ_u,

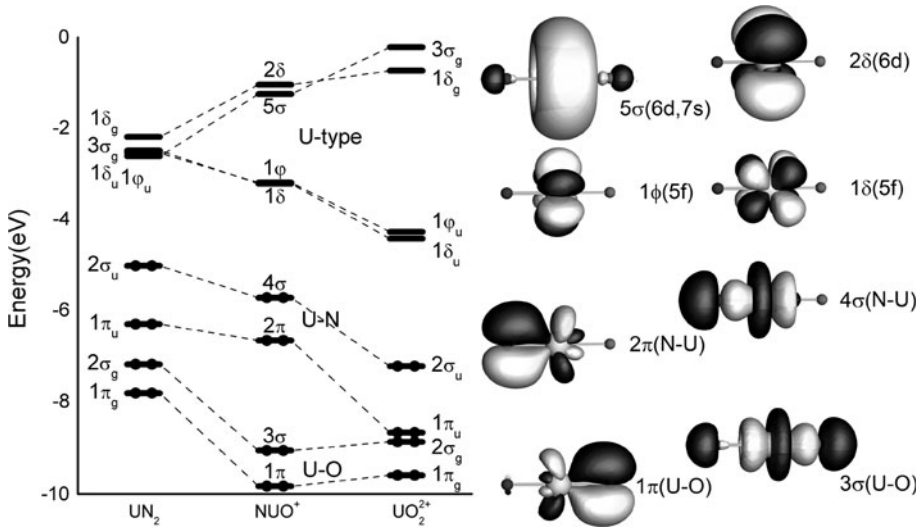

Fig. 1 Orbitals involved in electronic valence excitations (v) → U. *Left* Spectroscopic orbital energy (ε) level schemes ($\varepsilon_U - \varepsilon_v \approx \Delta E_{v\to U}$) of UN_2, NUO^+, and UO_2^{2+} (for DFT orbital energies, indicating also the active orbital spaces, see SI-Fig. 1). *Right* CMO envelops for NUO^+ (contour surface value 0.05 au)

U.5fδ_u, U.6dδ_g). We tried all possible selections, namely three (12,14) active spaces AS-dδ (with U.6dδ_g), AS-fδ (with U.5fδ_u) and AS-fϕ (with U.5fϕ_u), and three (12,16) active spaces AS-dδfδ (with U.6dδ_g and U.5fδ_u), AS-dδfϕ (with U.6dδ_g and U.5fϕ_u) and AS-fδfϕ (with U.5fδ_u and U.5fϕ_u). Such active spaces are consistent with those recommended by Pierloot for UO_2^{2+} [20] and seem sufficient for dealing with the low-lying excited states of the systems concerned. For UN_2, the mixing between the included and neglected configurations was shown to be small for nearly all electronic states.

In addition, we performed test calculations using CASSCF for selected states with parts of the semicore shells (U.6p, N.2s and O.2s) for 16 electrons in 16 active orbitals (excluding some of the U.6d and U.5f) and found that the energy of the first excited states changed by less than 0.2 eV. Therefore, the inclusion of the semicore shells in the CASSCF-based calculations does not have a significant contribution, when compared to the error bars of the methods.

For the SO-averaged and SO-coupled RAS calculations [36], the AS was partitioned into the bonding (RAS-I), the dominantly antibonding (RAS-II) and the intermediate non-bonding (RAS-III) regions. In these calculations, excitations from RAS-I were unrestricted, while RAS-II was allowed to be occupied by up to four electrons and RAS-III by one electron. To improve convergence, level shifts of 0.5–0.7 au were employed in the RASSCF calculations. Then, the second-order perturbation theory (PT2) corrections were determined. In all SO-RAS calculations using the 'state interaction' technique RAS-SI/SO, the diagonal elements of the SO matrices were replaced by the PT2 energies.

Extensive calculations were then carried out at different bond-lengths for the ground and excited states. The interatomic distances were varied in steps of 1 (or 2) pm, from 172 to 192 pm for U–N in UN_2 and from 170 to 188 pm for U–N and from 175 to 193 pm for U–O in NUO^+. The ground- and excited-state equilibrium distances, energies and harmonic vibrational force constants and frequencies were then obtained from quartic polynomial fittings. The resulting fit inaccuracy of the frequencies is of the order of 2%.

Relativistic DFT and TDDFT calculations were performed with the ADF 2009 program [37–39]. An all-electron quasi-relativistic ZORA Hamiltonian was used at the SO-averaged and SO-coupled levels [40, 41]. Exchange and correlation interactions were simulated for the ground state by DFT and for the excited states by TDDFT using the GGA-PW91 functional [42] and the asymptotically corrected SAOP functional [43, 44]. The 78 electrons in the U 1s-5d shells were kept frozen on the molecular ground-state potential surface. Uncontracted Slater type basis sets of polarized triple-zeta (TZP) and extensively polarized quadruple-zeta type (QZ4P) from the program library [45] were applied.

3 Explicitly correlated ab initio results

3.1 Ground states with spin-averaged Hamiltonian

Geometries and vibrational stretching frequencies are listed in Table 1. The bond lengths are reliable within about one pm. As expected, the U–N distance in UN_2 (175 pm) is slightly longer than the U–O one in UO_2^{2+} (171 pm). These

Table 1 UN_2, NUO^+, and UO_2^{2+}: ground-state properties of the free molecules

Molecule	Bond	CCSD(T)	RASPT2	CASPT2(*s*)[a]	CASPT2(*l*)[a]
(a) Bond length R_e (in Å)					
UN_2	U–N	1.743	1.758	1.751	1.735
NUO^+	U–N	1.703	1.714	1.710	1.695
	U–O	1.759	1.760	1.755	1.746
OUO^{2+}	U–O			1.714	1.705

Molecule	Mode	CCSD(T)	RASPT2	CASPT2(*s*)[a]	CASPT2(*l*)[a,b]	Exp[c]
(b) Harmonic frequencies ν_e (in cm^{-1})						
$^{238}U\ ^{14}N_2$	g	1,029	1,009	999	969 (1,015)	1,008
	u	1,075	1,066	1,064	1,031 (1,072)	1,077
$[^{14}N\ ^{238}U\ ^{16}O]^+$	'U–O'	962		1,023	942	970
	'U–N'	1,139		1,134	1,081	1,119
$[^{238}U\ ^{16}O_2]^{2+}$	g			1,043	959	
	u			1,153	1,066	

[a] CASPT2 calculations [17] with ANO-Small (*s*) or ANO-Large (*l*) MO sets

[b] In parentheses: including two g-AOs on U

[c] For more experimental information, see [4–9]

species can be viewed as having (nearly) triple-bonds between U,N and U,O. Indeed the distances are in the sum-range of Pyykkö's triple-bond covalent radii (172 pm for U–N, 171 pm for U–O) [46].

Interestingly, the bond lengths in NUO^+ are inverted, with a shorter U–N (170 pm) and a longer U–O (175 pm) distance, likely a *trans* effect. The averaged weighted effective atomic charges [47] of the three molecules are $[N^{-0.6}\ U^{+1.2}\ N^{-0.6}]^0$, $[N^{-0.4}\ U^{+1.7}\ O^{-0.3}]^{1+}$ and $[O^{-0.1}\ U^{+2.2}\ O^{-0.1}]^{2+}$. Remarkably, the negative charge on oxygen is a little smaller than that on nitrogen. Upon charging the triatomic complex by +1 unit, the negative charges on the ligands decrease somewhat, while the positive charge on the uranium increases more. The ionic attractions appear similar in UN_2 and NUO^+, but smaller in UO_2^{2+}. However, as shown below, the covalence of U−N is more pronounced than that of U−O, which may explain that U−N is shorter than U−O in NUO^+.

The wave numbers of the harmonic vibrations scatter by up to a few 10 cm^{-1}. The values calculated with large configuration spaces and basis sets agree reasonably well with the measured ones. Clearly, our one-electron basis sets without g-functions on U and f-functions on the ligands are not yet saturated. We have estimated the anharmonic reduction $vx = [10\ V'''^2/3\mu v^2 - V'''']/8\mu^2 v^2$ (in atomic units) from the quartic power fitting of $V(R_i - R_e)$, where V, μ, v, and R_i are the potential energy, effective mass, vibrational frequency and discretely varied internuclear distances, respectively; V''' and V'''' denote the third and fourth derivatives. For the gerade UN_2 stretching mode of the electronic ground state, we obtained a reduction by $vx = 22\ cm^{-1}$, which lies in the common range.

Table 2 presents the AO compositions of selected frontier canonical MOs (CMOs) at the DFT level. The AO populations of the σ, π and summed bonding MOs exhibit regular trends from UN_2 to NUO^+ to UO_2^{2+}, corresponding to the electronegativities of the three elements. The contributions from uranium increase from UO_2^{2+} to UN_2, indicating more covalent character in the U–N and less in the U–O bonds. In NUO^+, N wins against O in the competition for uranium AO participation in covalent bonding (see also 'excited states' below). The effective charges on U, N, and O indicate expectable charge transfers from U to N of about 0.4e, and from U to O of about 1.1e, when choosing a purely covalent picture with triple bonds as reference, $|E \equiv U \equiv E'|^{q+}$.

3.2 Excited states at the spin–orbit-averaged level

The SO-averaged SR-calculations provide us with a qualitative overview of the excited states. Table 3 displays our CASPT2 excitation energies of UN_2 along with those of isoelectronic UO_2^{2+} from the literature [20, 23, 24] and from our TDDFT calculations.

The results for different active orbital spaces (defined in Sect. 2) agree in most cases within several 0.01 eV up to about 0.2 eV. However, $1^1\Delta_g$ and $1^3\Delta_g$ vary a little more because of $(2\sigma_u^{-1}1\delta_u^1) - (1\pi_u^{-1}1\phi_u^1)$ mixing. Another exception is $2^1\Pi_u$ $(1\pi_g^{-1}\ 1\delta_u^1)$, due to its significant admixture (coefficient is 0.2) of doubly substituted configurations such as $(1\pi_u^{-1}\ 2\sigma_u^{-1}\ 1\delta_u^1 3\sigma_g^1)$. That is, most excitations of UN_2 are of the one-electron 'bonding HOMO (σ_u, π_u, σ_g, π_g)' → 'non-bonding LUMO (U.5fϕ_u, U.5fδ_u, U.6dδ_g, U.7 sσ_g)' type. They can be reproduced reasonably well with active spaces containing only one non-bonding orbital, fϕ, fδ or dδ or sσ. This generalizes the known rule of single U.5f population in the lowest excited states of UO_2^{2+}. Namely, CASPT2 energies obtained from AS-fϕfδ (listed in Table 3) and those from AS-fϕ or fδ are rather similar. The excited states of UN_2 can be well described by combining results from AS-fϕ, AS-fδ and AS-dδ calculations.

We applied such selections of active spaces for the SO-averaged CASPT2 and RASPT2 calculations of NUO^+, e.g. U.6dδ was not included in the AS for transitions to U.5fϕfδ. The results are displayed in Table 4. The RASPT2 results of UN_2 and UNO^+ in Tables 3 and 4 differ

Table 2 UN_2, NUO^+, and UO_2^{2+}: Atomic orbital compositions (in %) of the upper occupied bonding valence orbitals, from DFT calculations

Orbital	UN_2						UO_2^{2+}						Orbital	NUO^+							
	U				N[a]		U				O[a]			U				N		O	
	6p	5f	6d	7s	2s	2p	6p	5f	6d	7s	2s	2p		6p	5f	6d	7s	2s	2p	2s	2p
$2\sigma_u$	12	62	0	0	0	13	10	55	0	0	0	16	4σ	6	40	7	3	3	39	0	1
$1\pi_u$	0	42	0	0	0	28	0	33	0	0	0	33	2π	0	30	13	0	0	55	0	0
$2\sigma_g$	0	0	19	13	2	30	0	0	14	0	4	38	3σ	6	20	7	3	5	6	0	52
$1\pi_g$	0	0	33	0	0	33	0	0	19	0	0	40	1π	0	10	12	0	0	0	0	75
$\Sigma\sigma$	13	62	20	14	3	43	10	55	14	1	5	54	$\Sigma\sigma$	12	60	14	6	8	45	1	53
$\Sigma\pi$	0	42	33	0	0	61	0	33	19	0	0	74	$\Sigma\pi$	1	41	26	0	0	56	0	75
$\Sigma(\sigma+\pi)$	13	147	87	14	3	166	11	122	53	1	5	201	$\Sigma(\sigma+\pi)$	13	141	66	6	8	157	1	203

[a] Refers to one of the two equivalent atoms

Table 3 UN_2: Spin-averaged vertical excitation energies (in eV) at the SR-CAS/RAS-PT2 level for different active orbital spaces, at R(U–N) = 174.3 pm, and comparison with UO_2^{2+} (literature data and present SR-ZORA-TDDFT-SAOP results)

State[a]	Leading configuration	UN_2, CASSCF with different AS[b]				UO_2^{2+}			
		fδ or fϕ	dδ or f$\delta\phi$	dδfδ or dδfϕ	dδ/f$\delta\phi$ RASPT2	f$\delta\phi$ CASPT2[c]	CCSD[d]	TDDFT[e]	Present TDDFT
$1^3\Phi_g$	$2\sigma_u^{-1}1\varphi_u^1$	2.29	2.40	2.28	2.36	2.84	2.86	3.05	3.10
$\mathbf{1^1\Phi_g}$	$2\sigma_u^{-1}1\varphi_u^1$	2.80	2.91	2.79	2.86	3.37	3.42	3.50	3.54
$1^3\Delta_g$	$2\sigma_u^{-1}1\delta_u^1$	2.56	2.37	2.55	2.32	2.69	2.60	3.27	3.29
$\mathbf{1^1\Delta_g}$	$2\sigma_u^{-1}1\delta_u^1$	3.75	3.41	3.74	3.36	3.80	3.74	4.01	4.02
$a^3\Sigma_u^+$	$2\sigma_u^{-1}3\sigma_g^1$	2.61, 2.72	2.47, 2.54	2.40, 2.47	2.48				7.15
$a^1\Sigma_u^+$	$2\sigma_u^{-1}3\sigma_g^1$	2.82, 2.94	2.68, 2.75	2.67, 2.77	2.69				7.35
$1^3\Delta_u$	$2\sigma_u^{-1}1\delta_g^1$		3.02	2.92, 3.05	3.03				6.63
$1^1\Delta_u$	$2\sigma_u^{-1}1\delta_g^1$		3.21	3.13, 3.26	3.22				6.86
$1^3\Gamma_g$	$1\pi_u^{-1}1\varphi_u^1$	3.74	3.83	3.74	3.82	4.60	4.91	4.32	4.30
$1^1\Gamma_g$	$1\pi_u^{-1}1\varphi_u^1$	3.88	3.98	3.89	3.89	4.80	5.14	4.51	4.48
$2^3\Delta_g$	$1\pi_u^{-1}1\varphi_u^1$	3.75	3.84	3.75	3.82	4.62			4.29
$\mathbf{2^1\Delta_g}$	$1\pi_u^{-1}1\varphi_u^1$	4.09	4.30	4.09	4.22	4.92			4.86
$2^3\Phi_g$	$1\pi_u^{-1}1\delta_u^1$	3.96	3.95	3.99	3.94	4.55			4.66
$2^1\Phi_g$	$1\pi_u^{-1}1\delta_u^1$	3.99	4.00	4.01	3.93	4.54			4.66
$1^3\Pi_g$	$1\pi_u^{-1}1\delta_u^1$	3.97	3.97	4.00	3.94	4.56	4.84	4.70	4.66
$1^1\Pi_g$	$1\pi_u^{-1}1\delta_u^1$	4.13	4.12	4.14	4.03	4.80	4.81	4.99	4.89
$a^3\Pi_u$	$1\pi_u^{-1}3\sigma_g^1$	3.56, 3.63	3.42, 3.55	3.43, 3.51	3.41				8.29
$a^1\Pi_u$	$1\pi_u^{-1}3\sigma_g^1$	3.67, 3.74	3.55, 3.66	3.57, 3.65	3.54				8.38
$1^3\Phi_u$	$1\pi_u^{-1}1\delta_g^1$		4.01	3.94, 3.96	4.02				7.77
$1^1\Phi_u$	$1\pi_u^{-1}1\delta_g^1$		4.06	3.99, 4.07	4.07				7.84
$1^3\Pi_u$	$1\pi_u^{-1}1\delta_g^1$		4.05	3.98, 4.09	4.06				7.76
$1^1\Pi_u$	$1\pi_u^{-1}1\delta_g^1$		4.17	4.11, 4.22	4.18				7.99
$2^3\Phi_u$	$2\sigma_g^{-1}1\varphi_u^1$	4.46	4.61	4.57	4.51	4.73	4.97		4.26
$2^1\Phi_u$	$2\sigma_g^{-1}1\varphi_u^1$	4.53	4.68	4.65	4.57	4.76	5.04		4.34
$2^3\Delta_u$	$2\sigma_g^{-1}1\delta_u^1$	4.75	4.70	4.83	4.59	4.63	4.75		4.59
$2^1\Delta_u$	$2\sigma_g^{-1}1\delta_u^1$	4.74	4.70	4.93	4.57	4.55	4.70		4.60
$1^3\Gamma_u$	$1\pi_g^{-1}1\varphi_u^1$	5.31	5.37	5.37	5.34	5.50	6.09		4.93
$1^1\Gamma_u$	$1\pi_g^{-1}1\varphi_u^1$	5.30	5.38	5.41	5.32	5.43	6.01		4.92
$3^3\Delta_u$	$1\pi_g^{-1}1\varphi_u^1$	5.27	5.36	5.42	5.38	5.52			4.92
$3^1\Delta_u$	$1\pi_g^{-1}1\varphi_u^1$	5.32	5.27	5.37	5.36	5.45			4.98
$3^3\Phi_u$	$1\pi_g^{-1}1\delta_u^1$	5.21	5.31	5.48	5.32	5.21			4.93
$\mathbf{3^1\Phi_u}$	$1\pi_g^{-1}1\delta_u^1$	5.89	5.86	5.85	6.04	5.17			5.23
$2^3\Pi_u$	$1\pi_g^{-1}1\delta_u^1$	5.37	5.35	5.51	5.37	5.19	5.72		5.18
$2^1\Pi_u$	$1\pi_g^{-1}1\delta_u^1$	5.68	5.62	6.11	5.58	5.23	5.72		5.46

[a] A bold face singlet state indicates an unusually large singlet–triplet splitting

[b] The appropriate active orbital space(s) corresponding to the leading configuration of the term were chosen

[c] CASPT2, Pierloot et al. [20]

[d] IHFS-CCSD, Réal et al. [23]

[e] SOAP-SR-TDDFT, Réal et al. [24]

by less than 0.2 eV from CASPT2 with an average deviation <0.04 eV. However, there are two exceptional discrepancies of 0.3 and 0.7 eV for the $4^{1,3}\Delta$ ($1\pi^{-1}1\phi^1$) states of NUO^+, where the RASPT2 calculations encountered numerical difficulties.

The first and second excited states of UN_2 and UO_2^{2+} are $1^3\Delta_g$ ($2\sigma_u^{-1}$ $1\delta_u^1$) and $1^3\Phi_g$ ($2\sigma_u^{-1}1\phi_u{}^1$), and of NUO^+ are $1^3\Delta$ ($4\sigma^{-1}1\delta^1$) and $1^3\Phi$ ($4\sigma^{-1}$ $1\phi^1$). At higher energies, there follow manifolds of adjacent states, corresponding to (σ_u, π_u, σ_g, π_g) → (δ_u, ϕ_u, δ_g) excitations, see Figs. 1, 2 and 3. They begin around 2.3, 2.5 and 2.7 eV for UN_2, NUO^+, and UO_2^{2+}, respectively. In particular for the two symmetric molecules UN_2 and UO_2^{2+}, the excitations are of similar character. In all three cases, some of the excitations

Table 4 NUO^+: Spin-averaged vertical excitation energies (in eV) at the SR-CAS/RASPT2 level (see text, Sect. 3), at R(U–N) = 170.3 pm and R(U–O) = 175.9 pm

State	Leading configuration	Active space(s)	Vertical excitation energy	
			CASPT2	RASPT2
$1^3\Phi$	$4\sigma^{-1}1\varphi^1$	fϕ	2.52	2.54
$1^1\Phi$	$4\sigma^{-1}1\varphi^1$	fϕ	2.86	2.87
$1^3\Delta$	$4\sigma^{-1}1\delta^1$	fδ	2.40	2.46
$\mathbf{1^1\Delta}$	$4\sigma^{-1}1\delta^1$	fδ	3.19	3.20
$1^3\Gamma$	$2\pi^{-1}1\varphi^1$	fϕ	3.47	3.47
$1^1\Gamma$	$2\pi^{-1}1\varphi^1$	fϕ	3.57	3.57
$2^3\Delta$	$2\pi^{-1}1\varphi^1$	fϕ	3.47	3.47
$2^1\Delta$	$2\pi^{-1}1\varphi^1$	fϕ	3.73	3.73
$2^3\Phi$	$2\pi^{-1}1\delta^1$	fδ	3.54	3.53
$2^1\Phi$	$2\pi^{-1}1\delta^1$	fδ	3.59	3.59
$1^3\Pi$	$2\pi^{-1}1\delta^1$	fδ	3.54	3.54
$1^1\Pi$	$2\pi^{-1}1\delta^1$	fδ	3.81	3.81
$a^3\Sigma^+$	$4\sigma^{-1}5\sigma^1$	fδ, fϕ	4.57, 4.67	4.60
$a^1\Sigma^+$	$4\sigma^{-1}5\sigma^1$	fδ, fϕ	4.82, 4.95	4.87
$a^3\Pi$	$2\pi^{-1}5\sigma^1$	fδ, fϕ	5.30, 5.37	5.29
$a^1\Pi$	$2\pi^{-1}5\sigma^1$	fδ, fϕ	5.46, 5.51	5.46
$3^3\Phi$	$3\sigma^{-1}1\varphi^1$	fϕ	5.82	5.82
$3^1\Phi$	$3\sigma^{-1}1\varphi^1$	fϕ	5.93	5.93
$3^3\Delta$	$3\sigma^{-1}1\delta^1$	fδ	5.91	5.92
$3^1\Delta$	$3\sigma^{-1}1\delta^1$	fδ	6.11	6.12
$2^3\Gamma$	$1\pi^{-1}1\varphi^1$	fϕ	6.70	6.70
$2^1\Gamma$	$1\pi^{-1}1\varphi^1$	fϕ	6.70	6.69
$4^3\Delta$	$1\pi^{-1}1\varphi^1$	fϕ	6.72	6.04
$4^1\Delta$	$1\pi^{-1}1\varphi^1$	fϕ	6.73	6.41
$4^3\Phi$	$1\pi^{-1}1\delta^1$	fδ	6.58	6.60
$4^1\Phi$	$1\pi^{-1}1\delta^1$	fδ	6.58	6.60
$2^3\Pi$	$1\pi^{-1}1\delta^1$	fδ	6.59	6.60
$\mathbf{2^1\Pi}$	$2\pi^{-1}1\delta^1$	fδ	5.74	5.65

Singlets being more than 0.5 eV above their triplet mates are marked in bold face

into the 1δ MO are special in terms of their large singlet–triplet splittings of up to 1 eV, marked by bold face in Tables 3, 4 and 5.

In the case of UN_2, the 'U–N bonding ($2\sigma_u$,$1\pi_u$)' → 'U.7s-$3\sigma_g$' excitations are immersed in the lower energy region of 'U–N bonding → 'U.5f' excitations. For UNO^+, the corresponding excitations are about 2 eV higher, while those for UO_2^{2+} are expected even higher in energy. The formal, lowest antibonding orbital $3\sigma_g$ is mainly U.7s, strongly mixed with $6d_z^2$ (Fig. 1). The quasi-atomic U.7s-6d hybrid orbital becomes relatively destabilized from UN_2 ($3\sigma_g$) to NUO^+ (5σ) to UO_2^{2+} ($3\sigma_g$) with respect to the non-bonding U.5f levels upon increase of the total charge of the species (Fig. 1). Also the character of this lowest

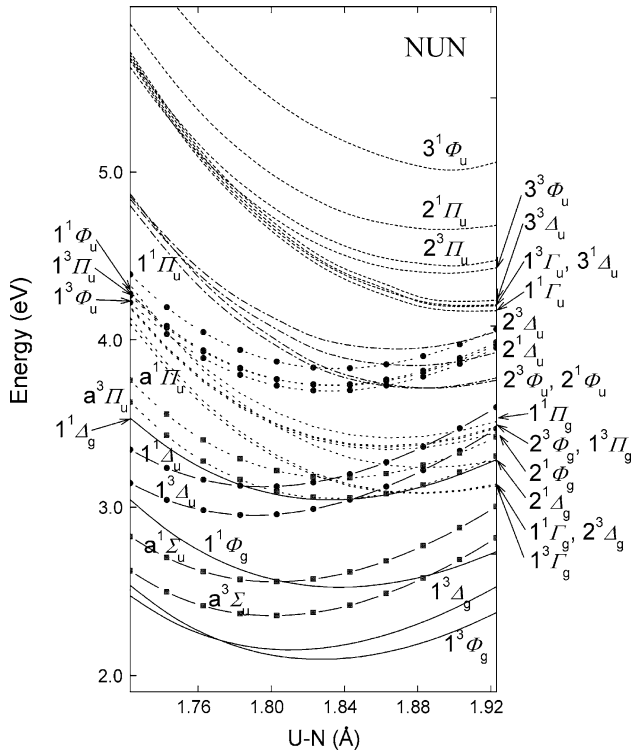

Fig. 2 Excited-state energy curves (in eV) of UN_2 along the symmetric U–N stretching mode (in Å) at the SO-averaged RASPT2 level. From *bottom* to *top*, *solid* $2\sigma_u$→U.5f; *long-dashed with squares* $2\sigma_u$→U.7 s; *long-dashed with heavy dots* $2\sigma_u$→U.6d; *dotted with squares* $1\pi_u$→U.7 s; *dotted* $1\pi_u$→U.5f; *dotted with heavy dots* $1\pi_u$→U.6d; *dash-dotted* $2\sigma_g$→U.5f; *dotted* $1\pi_g$→U.5f

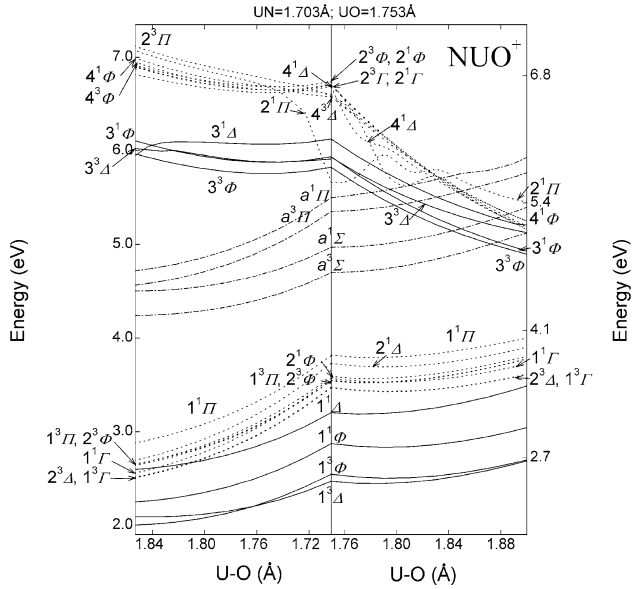

Fig. 3 Excited state energy curves (in eV) of NUO^+ versus the distances (in Å) of N–U and U–O (with the other bond length fixed) at the SO-averaged RASPT2 level. The central vertical line represents the equilibrium ground-state structure. From *bottom* to *top*, *solid* 4σ(N–U)→U.5f; *dotted* 2π(N–U)→U.5f; *dash-dotted* 4σ,2π(N–U)→U.7 s; *solid* 3σ(U–O)→U.5f; *dotted* 1π(U–O)→U.5f

Table 5 UN_2: Vertical electronic excitation energies E and adiabatic energy minima T_e (in eV), optimized U–N bond lengths R_e (in Å) and bond length expansions upon excitation Δ (in parentheses, in pm), harmonic vibrational symmetric stretching frequencies ν_e for ^{14}N (in cm^{-1})[a], from SR-RASPT2 calculations

State	Leading configuration	Active space	E	T_e	R_e (Δ)	ν_e[a]
$X^1\Sigma_g^+$		f$\delta\phi$	0	0	1.758	1,009
$1^3\Phi_g$	$2\sigma_u^{-1}1\varphi_u^1$	f$\delta\phi$	2.36	1.88	1.827 (6.9)	828
$1^1\Phi_g$	$2\sigma_u^{-1}1\varphi_u^1$	f$\delta\phi$	2.86	2.25	1.837 (7.9)	807
$1^3\Delta_g$	$2\sigma_u^{-1}1\delta_u^1$	f$\delta\phi$	2.32	2.02	1.811 (5.3)	841
$1^1\Delta_g$	$2\sigma_u^{-1}1\delta_u^1$	f$\delta\phi$	3.36	3.16	1.832 (7.4)	817
$a^3\Sigma_u^+$	$2\sigma_u^{-1}3\sigma_g^1$	f$\delta\phi$	2.48	2.28	1.801 (4.3)	867
$a^1\Sigma_u^+$	$2\sigma_u^{-1}3\sigma_g^1$	f$\delta\phi$	2.69	2.47	1.802 (4.4)	859
$1^3\Delta_u$	$2\sigma_u^{-1}1\delta_g^1$	dδ	3.03	2.91	1.791 (3.3)	850
$1^1\Delta_u$	$2\sigma_u^{-1}1\delta_g^1$	dδ	3.22	3.06	1.796 (3.8)	846
$1^3\Gamma_g$	$1\pi_u^{-1}1\varphi_u^1$	f$\delta\phi$	3.82	2.46	1.881 (12.3)	753
$1^1\Gamma_g$	$1\pi_u^{-1}1\varphi_u^1$	f$\delta\phi$	3.89	2.46	1.881 (12.3)	786
$2^3\Delta_g$	$1\pi_u^{-1}1\varphi_u^1$	f$\delta\phi$	3.82	2.48	1.879 (12.1)	780
$2^1\Delta_g$	$1\pi_u^{-1}1\varphi_u^1$	f$\delta\phi$	4.22	2.58	1.885 (12.7)	780
$2^3\Phi_g$	$1\pi_u^{-1}1\delta_u^1$	f$\delta\phi$	3.94	2.91	1.862 (10.4)	813
$2^1\Phi_g$	$1\pi_u^{-1}1\delta_u^1$	f$\delta\phi$	3.93	2.87	1.864 (10.6)	799
$1^3\Pi_g$	$1\pi_u^{-1}1\delta_u^1$	f$\delta\phi$	3.94	2.90	1.862 (10.4)	815
$1^1\Pi_g$	$1\pi_u^{-1}1\delta_u^1$	f$\delta\phi$	4.03	2.92	1.866 (10.8)	808
$a^3\Pi_u$	$1\pi_u^{-1}3\sigma_g^1$	f$\delta\phi$	3.41	2.81	1.835 (7.7)	863
$a^1\Pi_u$	$1\pi_u^{-1}3\sigma_g^1$	f$\delta\phi$	3.54	2.93	1.836 (7.8)	859
$1^3\Phi_u$	$1\pi_u^{-1}1\delta_g^1$	dδ	4.02	3.47	1.832 (7.4)	848
$1^1\Phi_u$	$1\pi_u^{-1}1\delta_g^1$	dδ	4.07	3.49	1.834 (7.6)	844
$1^3\Pi_u$	$1\pi_u^{-1}1\delta_g^1$	dδ	4.06	3.50	1.832 (7.4)	848
$1^1\Pi_u$	$1\pi_u^{-1}1\delta_g^1$	dδ	4.18	3.58	1.836 (7.8)	859
$2^3\Phi_u$	$2\sigma_g^{-1}1\varphi_u^1$	f$\delta\phi$	4.51	3.06	1.881 (12.3)	844
$2^1\Phi_u$	$2\sigma_g^{-1}1\varphi_u^1$	f$\delta\phi$	4.57	3.01	1.887 (12.9)	841
$2^3\Delta_u$	$2\sigma_g^{-1}1\delta_u^1$	f$\delta\phi$	4.59	3.41	1.868 (11.0)	852
$2^1\Delta_u$	$2\sigma_g^{-1}1\delta_u^1$	f$\delta\phi$	4.57	3.25	1.876 (11.8)	847
$1^3\Gamma_u$	$1\pi_g^{-1}1\varphi_u^1$	f$\delta\phi$	5.34	3.23	1.914 (15.6)	755
$1^1\Gamma_u$	$1\pi_g^{-1}1\varphi_u^1$	f$\delta\phi$	5.32	3.17	1.916 (15.8)	749
$3^3\Delta_u$	$1\pi_g^{-1}1\varphi_u^1$	f$\delta\phi$	5.38	3.20	1.918 (16.0)	733
$3^1\Delta_u$	$1\pi_g^{-1}1\varphi_u^1$	f$\delta\phi$	5.36	3.15	1.920 (16.2)	726
$3^3\Phi_u$	$1\pi_g^{-1}1\delta_u^1$	f$\delta\phi$	5.32	3.63	1.893 (13.5)	814
$3^1\Phi_u$	$1\pi_g^{-1}1\delta_u^1$	f$\delta\phi$	6.04	3.61	1.896 (13.8)	784
$2^3\Pi_u$	$1\pi_g^{-1}1\delta_u^1$	f$\delta\phi$	5.37	3.65	1.896 (13.8)	798
$2^1\Pi_u$	$1\pi_g^{-1}1\delta_u^1$	f$\delta\phi$	5.58	3.88	1.894 (13.6)	784

[a] The relaxed symmetric U–N bond-stretch force constant is $k_{r\text{-sym}}(U\text{–}N) = (\nu/348.2\ cm^{-1})^2$ N/cm

unoccupied σ-type orbital changes from non-bonding in UN_2 to weakly antibonding for UO_2^{2+}. This trend is consistent with that in the isoelectronic series CUO, NUO^+, UO_2^{2+} [18]. It is also consistent with the remarkable ground state reversal of UO_2 and CUO upon implementation into a noble-gas matrix [48, 49].

A special character of the excited states of NUO^+ is the energetic separation of two groups of excitations: at lower energies, the excitations out of the U–N bonding 4σ and 2π MOs and at higher energies the excitations out of the U–O bonding 3σ and 1π MOs. The $1^{1,3}\Delta$ ($4\sigma^{-1}1\sigma^1$) singlet–triplet splitting of 0.79 eV is anomalously large, the one of $2^{1,3}\Pi$ ($1\pi^{-1}1\delta^1$) of −0.95 eV even of opposite sign. This is due to a 30% mixing with (2π,$4\sigma \rightarrow$ U.5fϕfδ,U.7sσ) doubly substituted configurations.

We have determined bond stretching energy curves for UN_2 and NUO^+ by RASPT2 (Figs. 2 and 3; for UO_2^{2+} see [20]). The energy minima (adiabatic transition energies T_e), equilibrium bond lengths (R_e), bond length expansions upon electronic excitation (Δ) and harmonic symmetric-stretching vibrational frequencies ν (for UN_2) or unrelaxed bond stretching force constants k_{un} (for UNO^+) are displayed in Tables 5 and 6. A large Δ goes along with a reduced ν or k. For the largest Δ values of UN_2, k is reduced to nearly one half; for the largest Δ(U–N) and Δ(U–O) values of UNO^+, k_{un}(U–N) may be reduced to one sixth and k_{un}(U–O) to one third.

The electronic excitations from occupied bonding MOs '***a***' to non-bonding or weakly antibonding orbitals '***b***' cause bond length expansions $\Delta_{a\rightarrow b}$(U–N) or $\Delta_{a\rightarrow b}$(U–O) from a few pm up to nearly 40 pm. The $\Delta_{a\rightarrow b}$ values can be approximated by orbital increments, $\Delta_{a\rightarrow b} \approx \Delta_a - \Delta_b$, where Δ_a and Δ_b are measures of the bond contracting powers of an electron in occupied orbital ***a*** and in excited orbital ***b***. The orbital increments are listed in Table 7a. In all three molecules, excitations to U.5fδ_u are energetically a little lower than to U.5f-ϕ_u. In UN_2 (or UO_2^{2+}), all the upper occupied valence MOs $2\sigma_u$, $2\sigma_g$, $1\pi_u$ and $1\pi_g$ are U–N (or U–O bonding). In NUO^+, however, the orbitals are localized on either the U–N or on the U–O unit (see Fig. 1). According to Table 7a, the 1π and 3σ MOs are strongly U–O bonding and weakly U–N bonding, while the 2π and 4σ MOs are strongly U–N bonding and weakly U–O bonding. Another measure of the bonding power of an orbital is its energy slope with respect to the internuclear distance [50, 51]. Respective $\partial\varepsilon/\partial R$ values are listed in Table 7b as well, which show a similar pattern as the Δ increments.

Excitations from the localized bonds in NUO^+ cause not only large expansions of bond length and reductions of force constant but also large vertical-adiabatic energy differences $\Delta E_{v\rightarrow a}$, when compared to the symmetric molecules UN_2 and UO_2^{2+} with delocalized canonical orbitals. For example, the ΔE_{v-a} values of the lowest excited states $1^3\Delta$ and $1^3\Phi$ of UNO^+ are 0.7 and 1 eV, while they are only 0.3 and 0.5 eV for UN_2. Overall, there is some similarity of the U–N excited states of NUO^+ with the lower excited states of UN_2 and of the U–O excited states of NUO^+ with the higher excited states of UO_2^{2+}. The different MO level schemes are reflected in the spectra (see

Table 6 NUO^+: SO-averaged SR vertical electronic excitation energies E and adiabatic energy minima T_e [a] (in eV), optimized bond lengths R_e [a] (in Å) and bond length expansions upon excitation Δ (in parentheses, in pm), and harmonic unrelaxed stretching force constants k_{un} [a] (in N/cm), from SR-RASPT2 calculations

SR state	Leading configuration	Active space	E	T_e	R_e(U–N) and (Δ)	k_{un} (U–N)	R_e(U–O) and (Δ)	k_{un} (U–O)
$X^1\Sigma^+$		fϕ	0	0	1.714	8.82	1.760	7.48
$1^3\Phi$	$4\sigma^{-1}1\varphi^1$	fϕ	2.54	1.51	1.866 (15.2)	4.95	1.795 (3.5)	6.65
$1^1\Phi$	$4\sigma^{-1}1\varphi^1$	fϕ	2.87	1.64	1.883 (16.9)	4.43	1.792 (3.2)	6.69
$1^3\Delta$	$4\sigma^{-1}1\delta^1$	fδ	2.46	1.76	1.842 (12.8)	4.97	1.782 (2.2)	6.70
$1^1\Delta$	$4\sigma^{-1}1\delta^1$	fδ	3.20	1.96	1.895 (18.1)	4.12	1.772 (1.2)	6.81
$1^3\Gamma$	$2\pi^{-1}1\varphi^1$	fϕ	3.47	1.32	1.959 (24.5)	2.31	1.794 (3.4)	6.34
$1^1\Gamma$	$2\pi^{-1}1\varphi^1$	fϕ	3.57	1.17	1.986 (27.2)	1.30	1.793 (3.3)	6.47
$2^3\Delta$	$2\pi^{-1}1\varphi^1$	fϕ	3.47	1.35	1.956 (24.2)	2.47	1.795 (3.5)	6.34
$2^1\Delta$	$2\pi^{-1}1\varphi^1$	fϕ	3.73	1.27	1.990 (27.6)	1.19	1.790 (3.0)	6.65
$2^3\Phi$	$2\pi^{-1}1\delta^1$	fδ	3.54	1.72	1.934 (22.0)	3.73	1.777 (1.7)	6.86
$2^1\Phi$	$2\pi^{-1}1\delta^1$	fδ	3.59	1.66	1.941 (22.7)	2.97	1.777 (1.7)	6.73
$1^3\Pi$	$2\pi^{-1}1\delta^1$	fδ	3.54	1.75	1.932 (21.8)	3.65	1.777 (1.7)	6.84
$1^1\Pi$	$2\pi^{-1}1\delta^1$	fδ	3.81	1.89	1.942 (22.8)	2.79	1.777 (1.7)	6.51
$3^3\Phi$	$3\sigma^{-1}1\varphi^1$	fϕ	5.82	3.52	1.753 (3.9)	8.18	2.029 (26.9)	2.86
$3^1\Phi$	$3\sigma^{-1}1\varphi^1$	fϕ	5.93	3.52	1.750 (3.6)	8.28	2.025 (26.5)	3.65
$3^3\Delta$	$3\sigma^{-1}1\delta^1$	fδ	5.92	4.05	1.745 (3.1)	8.96	2.004 (24.4)	2.91
$3^1\Delta$	$3\sigma^{-1}1\delta^1$	fδ	6.12	4.01			2.012 (25.2)	4.07
$2^3\Gamma$	$1\pi^{-1}1\varphi^1$	fϕ	6.70	3.14	1.747 (3.3)	8.34	2.075 (31.5)	3.71
$2^1\Gamma$	$1\pi^{-1}1\varphi^1$	fϕ	6.69	3.19	1.745 (3.1)	8.41	2.065 (30.5)	4.30
$4^3\Delta$	$1\pi^{-1}1\varphi^1$	fϕ	6.04	2.39	1.751 (3.7)	8.25	2.145 (38.5)	2.78
$4^1\Delta$	$1\pi^{-1}1\varphi^1$	fϕ	6.41	2.49	1.746 (3.2)	8.24	2.121 (36.1)	4.26
$4^1\Phi$	$1\pi^{-1}1\delta^1$	fδ	6.60	3.22	1.737 (2.3)	8.58	2.112 (35.2)	4.59
$4^3\Phi$	$1\pi^{-1}1\delta^1$	fδ	6.60	3.64	1.736 (2.2)	8.71	2.051 (29.1)	1.70
$2^3\Pi$	$1\pi^{-1}1\delta^1$	fδ	6.60	3.71			2.045 (28.5)	4.40
$2^1\Pi$	$1\pi^{-1}1\delta^1$	fδ	5.65					

[a] Only one of the two bond lengths is varied for each case, with the other bond length fixed

Table 7 UN_2, NUO^+, and UO_2^{2+}: valence and virtual orbital characteristics

Molecule[a]	Bond	$1\pi_g$, 1π	$2\sigma_g$, 3σ	$1\pi_u$, 2π	$2\sigma_u$, 4σ	U.5f-δ_u, U.5f-δ	U.5f-ϕ_u, U.5f-ϕ	U.7s-σ_g, U.7s-σ	U.6d-δ_g, U.6d-δ
NUN	U–N	15.7	12.6	11.9	7.4	1.8	0	3.6	4.3
NUO^+	U–N	3.5	4.3	23.2	15.7	1.7	0	3.0	
	U–O	35.9	31.2	8.0	8.5	2.0	0	4.9	
OUO^{2+}	U–O	17.9	11.8	14.7	7.7	1.9	0		

Molecule[b]	Bond	$1\pi_g$, 1π	$2\sigma_g$, 3σ	$1\pi_u$, 2π	$2\sigma_u$, 4σ	Sum of OMOs	U.5f-δ_u, U.5f-δ	U.5f-ϕ_u, U.5f-ϕ	U.7s-σ_g, U.7s-σ	U.6d-δ_g, U.6d-δ
NUN	U–N	5.6	4.0	4.9	3.5	28.5	0.7	0	3.3	2.6
NUO^+	U–N	0.8	0.3	9.6	6.4	27.5	0.7	0	3.3	2.6
	U–O	12.5	6.8	0.6	0.6	33.6	0.9	0	1.3	1.5
OUO^{2+}	U–O	7.0	4.2	6.2	3.8	34.4	0.8	0	1.0	1.1

[a] Increments Δ (in pm) of bond-contracting power of an electron in various orbitals **a**, **b**, fitted to the geometries of the excited states of type a→b, relative to U.5fϕ

[b] Slopes $\partial\varepsilon/\partial R$ (in eV/Å) of ground-state DFT orbital energies ε upon expansion of bond length R, relative to the $\partial\varepsilon/\partial R$ values of U.5fϕ. The four absolute $\partial\varepsilon/\partial$R values of U.5f$\phi$ for NUN to OUO^{2+} are −3.0, −2.4, −3.2, −2.2 eV/Å

Table 8 UO_2^{2+}: Lowest SO-coupled excited states, principal SR component, and vertical excitation energies E (in cm^{-1}) from (Atomic-Mean-Field) AMF-SO-CAS(12,16)(l) [20] and RECP-SO-RAS (this work)

SO state	Principal SR state	E	
		AMF-SO-CAS (12,16) (l)	RECP-SO-RAS
$a\Delta_g$	$1^3\Phi_g$ ($2\sigma_u^{-1}1\varphi_u^1$)	19,195	19,118
$a\Pi_g$	$1^3\Delta_g$ ($2\sigma_u^{-1}1\delta_u^1$)	20,104	20,116
$a\Phi_g$	$1^3\Phi_g$ ($2\sigma_u^{-1}1\varphi_u^1$)	20,265	20,253
$b\Delta_g$	$1^3\Delta_g$ ($2\sigma_u^{-1}1\delta_u^1$)	22,320	22,377
$b\Phi_g$	$1^3\Delta_g$ ($2\sigma_u^{-1}1\delta_u^1$)	25,435	25,653
$a\Gamma_g$	$1^3\Phi_g$ ($2\sigma_u^{-1}1\varphi_u^1$)	26,312	26,557
$c\Phi_g$	$1^1\Phi_g$ ($2\sigma_u^{-1}1\varphi_u^1$)	29,085	29,345
$c\Delta_g$	$1^1\Delta_g$ ($2\sigma_u^{-1}1\delta_u^1$)	31,314	31,405
$b\Pi_g$	$2^3\Delta_g$ ($1\pi_u^{-1}1\varphi_u^1$)	32,921	32,576
$b\Gamma_g$	$1^3\Gamma_g$ ($1\pi_u^{-1}1\varphi_u^1$)	33,262	33,104

the lower middle and right parts of the level scheme of Fig. 1).

3.3 Spin–orbit-coupled excited states

As a test, we performed calculations on UO_2^{2+} with the RAS-SI/SO approach on top of SR-RASPT2. The results in Table 8 differ from Pierloot's SO-CASPT2 results by less than 0.04 eV, and on the average by less than 0.02 eV. Therefore, we also applied this approach to UN_2 and UNO^+. Table 9 lists the SO-coupled excited states of type ($1\sigma_u$,$1\pi_u$) → (U.5fδ_u,ϕ_u), their vertical excitation energies and the dominant SR $^{2S+1}\Lambda_p$ term contributions. The large SO coupling of the U.5f orbital causes significant splittings. The splittings are slightly larger for the U.5f-ϕ_u excited states than for the U.5f-δ_u ones, owing to the larger angular momentum coupling for the U.5fϕ_u. For instance, the lowest SO-coupled $1\Delta_g$ states are stabilized with respect to

Table 9 UN_2: Excited SO-coupled states in terms of SO-averaged SR states at R(U–N) = **174** pm

SO state	Vertical excitation energy (eV)	Component of SR states (%)[a]											
		$\sigma_u^{-1}\delta_u^1$		$\sigma_u^{-1}\phi_u^1$		$\pi_u^{-1}\delta_u^1$				$\pi_u^{-1}\phi_u^1$			
		$1^3\Delta_g$	$1^1\Delta_g$	$1^3\Phi_g$	$1^1\Phi_g$	$1^3\Pi_g$	$2^3\Phi_g$	$1^1\Pi_g$	$2^1\Phi_g$	$2^3\Delta_g$	$1^3\Gamma_g$	$2^1\Delta_g$	$1^1\Gamma_g$
$1\Delta_g$	1.89	15	2.7	**79**									
$1\Phi_g$	2.03	20		**55**	20								
$1\Pi_g$	2.10	**97**				1.9		1.0					
$2\Delta_g$	2.36	**77**	6.7	12									
$2\Phi_g$	2.73	**72**		25			1.6						
$1\Gamma_g$	2.75			**98**									2.4
$3\Phi_g$	3.07	4.8		17	**69**					4.6	4.2		
$2\Pi_g$	3.27							5.6		**90**			
$2\Gamma_g$	3.29						12				**50**		37
$3\Delta_g$	3.37		**67**	7.6		12				8.5			
$4\Phi_g$	3.54				3.5		**44**		11		41		
$1\Sigma_g$	3.65					**99**							
$5\Phi_g$	3.63				3.0		11		**45**		40		
$4\Delta_g$	3.79		4.7				24			**57**		11	
$5\Delta_g$	3.95		11				**64**			23			
$3\Pi_g$	3.98	2.8				**76**		20					
$6\Phi_g$	4.11										**100**		
$3\Gamma_g$	4.23						**87**				5.1		7.8
$4\Pi_g$	4.29					17		**73**		9.2			
$6\Delta_g$	4.41					5.1	5.2			4.6		**84**	
$7\Phi_g$	4.39			1.8	3.6					**94**			
$4\Gamma_g$	4.46			3.4							43		**53**
$7\Delta_g$	4.49	2.0	7.1			**81**				6.0		2.9	
$8\Phi_g$	4.51	2.8					**43**		42		11		

[a] The percentage of the main $n^{2S+1}\Lambda_p$ term is given in bold face

their SR $^3\Phi_u$ origin by 4,151 cm^{-1} in UN_2 and by 4,494 cm^{-1} in UO_2^{2+}. That is, the lowest excited states have now dominant U.5fϕ character due to SO splitting in all three molecules.

The first excitation from ungerade orbitals to U.7s-3σ_g, $1\Sigma_u^-$ ($a^3\Sigma_u$, $\sigma_u^{-1}\sigma_g^1$) at 2.48 eV, shows a minor SO effect, while the first excitation to U.6d-δ_g, $2\Pi_u$ ($1^3\Delta_u$, $2\sigma_u^{-1}1\delta_g^1$) at 2.75 eV, shows an intermediate SO coupling (Table 10). The SO shifts of the states can be qualitatively estimated from the SO coupling constants of the respective atomic orbitals.

The UN_2 energy curves for both gerade and underage states up to 3.8 eV are plotted in Fig. 4. Several avoided crossings are visible, which are not easy to handle computationally. The RAS-SI/SO calculations of excitations to the U.5fδ,fϕ, the U.6dδ, and the U.7sσ orbitals show that there is no strong mixing by SO coupling between these three types of excited states. The SR $^{2S+1}\Lambda_p$ origins, vertical and adiabatic excitation energies, equilibrium bond lengths, bond expansions, harmonic symmetric stretching frequencies, and the SO contributions are listed in Table 10. In a few cases, the SO coupling changes the bond lengths by more than one pm, and the frequencies by more than 5%, though changes up to 30% occur, too. Overall, the various excitations to U.5fδfϕ in the visible and near-UV are similar for UN_2 and UO_2^{2+}. However, while excitations to U.6dδ and U.7sσ overlap with those to U.5fδfϕ for UN_2, they are all expected above the valence to U.5f manifold for UO_2^{2+}, according to the optical orbital level diagram of Fig. 1.

Results for NUO^+ are presented in Table 11 and Fig. 5. Several avoided state crossings are again visible, being accompanied by strongly varying configuration mixings along the bond energy curves. Therefore, not all possible states could be determined with sufficient accuracy. Again, the structure of the spectrum is governed by lower energy excitations from the U–N bonding MOs 4σ and 2π, and by higher energy excitations from the U–O bonding MOs 3σ and 1π. Large SO splittings are determined by the final U.5f MOs. For instance, the lowest SO-coupled U–N and U–O bond excitations (with their SR origins) are, respectively, $a1\Delta$ at 2.03 eV ($1^3\Phi$, $4\sigma^{-1}1\varphi^1$ at 2.54 eV) and $b1\Delta$ at 5.32 eV ($3^3\Phi$, $3\sigma^{-1}1\varphi^1$ at 5.82 eV). Their SO stabilizations are very similar, 0.51 and 0.50 eV.

Table 10 UN_2: SO-coupled electronic states, originating from SO-averaged SR states, vertical and adiabatic excitation energies E and T_e (in eV), optimized bond lengths R_e (in Å), bond length expansions Δ upon excitation and (in parentheses) its SO coupling contributions $\delta_{SO}\Delta$ (in pm), harmonic symmetric stretching frequencies ν_e for ^{14}N and (in parentheses) its SO coupling contributions $\delta_{SO}\nu$ (in cm^{-1})

SO state	Principal SR state	E	T_e	R_e	Δ ($\delta_{SO}\Delta$)[a]	ν_e ($\delta_{SO}\nu$)[a]
X Σ_g^+				1.759		981 (−28)
$1\Delta_g$	$1^3\Phi_g$	1.89	1.39	1.825	6.6 (−0.3)	821 (−7)
$1\Phi_g$	$1^3\Phi_g$	2.03	1.51	1.827	6.8 (−0.1)	819 (−9)
$1\Pi_g$	$1^3\Delta_g$	2.10	1.74	1.812	5.3 (0.0)	830 (−9)
$2\Delta_g$	$1^3\Delta_g$	2.36	1.99	1.813	6.6 (**+1.3**)	837 (−4)
$1\Sigma_u^-$	$a^3\Sigma_u^+$	2.48	2.20	1.802	4.3 (0.0)	864 (−3)
$1\Pi_u$	$a^3\Sigma_u^+$	2.48	2.21	1.802	4.3 (0.0)	865 (−2)
$1\Sigma_u^+$	$a^1\Sigma_u^+$	2.67	2.38	1.804	4.5 (+0.1)	853 (−6)
$2\Phi_g$	$1^3\Delta_g$	2.73	2.35	1.813	5.4 (+0.1)	852 (+11)
$1\Gamma_g$	$1^3\Phi_g$	2.75	2.20	1.830	7.1 (+0.2)	762 (**−66**)
$2\Pi_u$	$1^3\Delta_u$	2.75	2.62	1.794	3.5 (+0.2)	837 (−13)
$1\Delta_u$	$1^3\Delta_u$	2.82	2.68	1.795	3.6 (+0.3)	842 (−8)
$3\Phi_g$	$1^1\Phi_g$	3.07	2.33	1.847	8.8 (+0.9)	708 (**−99**)
$1\Phi_u$	$1^3\Delta_u$	3.16	3.05	1.791	3.2 (−0.1)	845 (−5)
$2\Delta_u$	$1^1\Delta_u$	3.26	3.15	1.791	3.2 (−0.6)	827 (−19)
$2\Pi_g$	$2^3\Delta_g$	3.27	2.01	1.873	11.4 (−0.7)	797 (+17)
$2\Gamma_g$	$1^3\Gamma_g$	3.29	2.12	1.862	10.3 (**−2.0**)	949 (−4)
$3\Delta_g$	$1^1\Delta_g$	3.37	2.24	1.874	11.5 (**+4.1**)	631 (**−186**)
$3\Delta_u$	$a^3\Pi_u$	3.49	2.91	1.832	7.3 (−0.4)	864 (+1)
$3\Pi_u$	$a^3\Pi_u$	3.50	2.80	1.832	7.3 (−0.4)	877 (+14)
$4\Phi_g$	$2^3\Phi_g$	3.54	2.37	1.864	10.5 (+0.1)	888 (**+75**)
$2\Phi_u$	$1^3\Phi_u$	3.72	3.04	1.836	7.3 (−0.3)	861 (+13)

[a] Comparatively large values in bold face

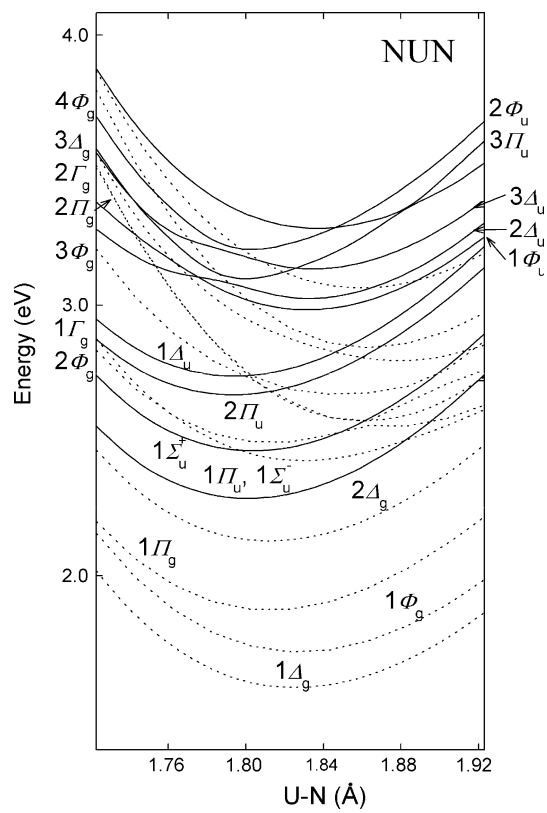

Fig. 4 Excited state energy curves (in eV) of UN_2 along the symmetric U–N stretching mode (in Å) at the SO-coupled RASPT2 level. *Dotted* gerade states; *solid* ungerade states

Table 11 NUO^+: Some of the SO-coupled electronic states, originating from SO-averaged SR states

SO state[a]	Principal SR state	E	SO state	Principal SR state	E
a					
$X\Sigma^+$	$1\Sigma^+$		$b1\Delta$	$3^3\Phi$	5.32
$a1\Delta$	$1^3\Phi$	2.03	$b1\Phi$	$3^3\Phi$	5.36
$a1\Phi$	$1^3\Phi$	2.13	$b1\Pi$	$3^3\Delta$	5.64
$a1\Pi$	$1^3\Delta$	2.19	$b2\Delta$	$3^3\Delta$	5.74
$a2\Delta$	$1^3\Delta$	2.43	$b1\Gamma$	$2^3\Gamma$	6.12
$a2\Phi$	$1^3\Delta$	2.84	$b2\Pi$	$4^3\Delta$	6.15
$a1\Gamma$	$1^3\Phi$	2.87	$b2\Gamma$	$3^3\Phi$	6.20
$a2\Pi$	$2^3\Delta$	2.92	$b2\Phi$	$3^1\Phi$	6.20
$a2\Gamma$	$1^3\Gamma$	2.97	$b3\Phi$	$3^3\Delta$	6.26
$a3\Phi$	$1^1\Phi$	3.03	$b3\Delta$	$4^3\Delta$	6.27
$a3\Delta$	$1^1\Delta$	3.08	$b4\Phi$	$2^3\Gamma$	6.29
…	…	…	$b4\Delta$	$4^3\Phi$	6.30
			$b5\Phi$	$4^1\Phi$	6.33
			$b5\Delta$	$1^1\Delta$	6.39

SO state[b]	Principal SR state	E	T_e	R_e(UN) and (Δ)	$\delta_{SO}\Delta_{UN}$	k_{un}(UN)	$\delta_{SO}k$(UN)
b							
$X\Sigma^+$	$1\Sigma^+$			1.716	+0.2	8.22	−0.60
$a1\Delta$	$1^3\Phi$	2.03	1.02	1.867 (15.0)	+0.1	4.29	−0.66
$a1\Phi$	$1^3\Phi$	2.13	1.12	1.865 (14.8)	−0.1	4.91	−0.04
$a1\Pi$	$1^3\Delta$	2.19	1.05	1.901 (19.1)	+5.9	1.21	−3.76
$a2\Delta$	$1^3\Delta$	2.43	1.53	1.861 (14.4)	+1.9	5.41	+0.44
$a2\Phi$	$1^3\Delta$	2.84	1.47	1.881 (17.5)	+3.9	7.63	+2.66
…	…	…	…	…	…	…	…
				R_e(UO)	$\delta_{SO}\Delta_{UO}$	k_{un} (UO)	$\delta_{SO}k$(UO)
$X\Sigma^+$	$1\Sigma^+$			1.763	+0.3	7.80	+0.32
$b1\Delta$	$3^3\Phi$	5.32	2.93	2.053 (29.3)	+2.4	2.50	−0.36
$b1\Phi$	$3^3\Phi$	5.36	2.99	2.043 (28.3)	+1.4	3.22	+0.36

[a] Vertical excitation energies E (in eV). Left section for U–N valence orbital excitations, right section for U–O valence orbital excitations

[b] Vertical and adiabatic excitation energies E and T_e (in eV); optimized U–N and U–O bond lengths R_e (in Å) for the other bond being held fixed, and respective bond length expansions Δ (in parentheses, in pm) upon electronic excitation, with respect to the ground-state reference values of 171 pm (U–N) and 176 pm (U–O); SO coupling contribution $\delta_{SO}\Delta$ (in pm) to Δ; unrelaxed harmonic bond stretching force constants k_{un} (in N/cm); and changes $\delta_{SO}k$ (in N/cm) due to SO coupling. Upper section for U–N valence orbital excitations, lower section for U–O valence orbital excitations

Remarkably, the SO corrections of bond lengths (denoted as $\delta_{SO}R$) and force constants (denoted as $\delta_{SO}k$) of NUO^+ are significantly larger than those for the other two symmetric molecules. For our selection of excited states, the $\delta_{SO}R$ values lie within 1–6 pm, in most cases SO bond lengthening. Concerning the force constants, $\delta_{SO}k$ for U–O is 20% on the average (up to 50%), and $\delta_{SO}k$ for U–N is 65% on the average (up to 175%). One may argue that the excitation from a localized bonding orbital in UNO^+ makes that bond softer and more susceptible to SO perturbations. Furthermore, the localized electron hole on one side of the molecule will polarize the final orbital in the excited state and that may be the reason for more pronounced SO-induced configuration mixing in NUO^+.

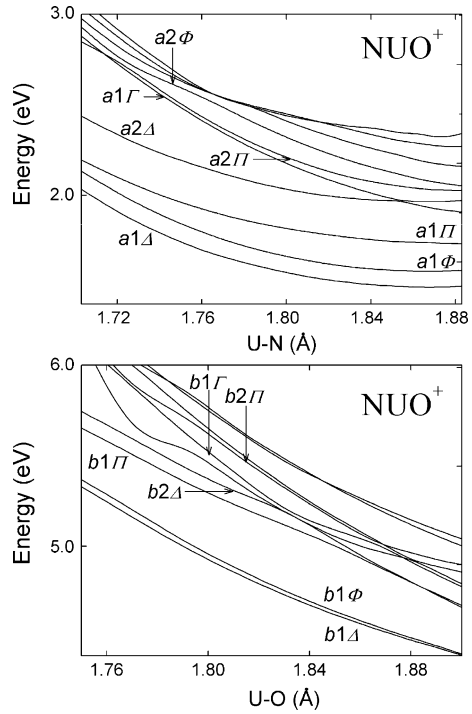

Fig. 5 Excited-state energy curves (in eV) of NUO^+ at the SO-coupled RASPT2 level versus bond lengths (in Å). *Top* N–U-bond excited states versus N–U distance; *bottom* higher U–O bond excited states versus U–O distance

4 Density functional results

Since multi-reference ab initio electron correlation calculations are computationally demanding, TDDFT for the excited states of actinide compounds is potentially an important alternative. We compare our ab initio data in Tables 12, 13, and 14 with TDDFT results for two different XC functionals. Table 12 presents vertical SR excitation energies for UN_2. Excitations to the U.7sσ_g and U.6dδ_g MOs are reasonably well reproduced concerning both the energy values and their energetic order. The radial distributions of the medium U.6d and extended U.7s AOs allow for appreciable overlap with the U–N/O bonding orbitals [26, 27, 52].

On the other hand, the DFT results for the excitations to the U.5fδ_u, fϕ_u MOs are less satisfactory, with the order of levels above 3 eV being rather 'statistical' and energy

Table 12 UN_2: Vertical excitation energies (in eV) at the SR level from TDDFT using exchange-correlation potentials PW91 or SAOP and basis sets TZ2P or QZ4P, compared to CASPT2

SR state	Leading configuration	TDDFT PW91/ZTP	TDDFT SAOP/TZP	TDDFT SAOP/QZ4P	CASPT2
$1^3\Delta_g$	$2\sigma_u^{-1}1\delta_u^1$	1.71	2.48	2.43	2.37
$1^3\Phi_g$	$2\sigma_u^{-1}1\varphi_u^1$	1.03	2.02	1.93	2.40
$a^3\Sigma_u^+$	$2\sigma_u^{-1}3\sigma_g^1$	2.36	2.62	2.58	2.54
$a^1\Sigma_u^+$	$2\sigma_u^{-1}3\sigma_g^1$	2.61	2.86	2.83	2.75
$1^1\Phi_g$	$2\sigma_u^{-1}1\varphi_u^1$	1.47	2.45	2.36	2.91
$1^3\Delta_u$	$2\sigma_u^{-1}1\delta_g^1$	3.09	3.21	3.22	3.02
$1^1\Delta_u$	$2\sigma_u^{-1}1\delta_g^1$	3.23	3.40	3.39	3.21
$1^1\Delta_g$	$2\sigma_u^{-1}1\delta_u^1$	2.27	3.03	2.97	3.41
$a^3\Pi_u$	$1\pi_u^{-1}3\sigma_g^1$	3.48	3.52	3.49	3.55
$a^1\Pi_u$	$1\pi_u^{-1}3\sigma_g^1$	3.60	3.65	3.62	3.66
$1^3\Gamma_g$	$1\pi_u^{-1}1\varphi_u^1$	2.21	2.99	2.91	3.83
$2^3\Delta_g$	$1\pi_u^{-1}1\varphi_u^1$	2.21	2.99	2.91	3.84
$2^3\Phi_g$	$1\pi_u^{-1}1\delta_u^1$	3.04	3.62	3.56	3.95
$1^3\Pi_g$	$1\pi_u^{-1}1\delta_u^1$	3.04	3.61	3.56	3.97
$1^1\Gamma_g$	$1\pi_u^{-1}1\varphi_u^1$	2.42	3.18	3.09	3.98
$2^1\Phi_g$	$1\pi_u^{-1}1\delta_u^1$	3.05	3.62	3.57	4.00
$1^3\Phi_u$	$1\pi_u^{-1}1\delta_g^1$	4.15	4.15	4.16	4.01
$1^3\Pi_u$	$1\pi_u^{-1}1\delta_g^1$	4.15	4.14	4.15	4.05
$1^1\Phi_u$	$1\pi_u^{-1}1\delta_g^1$	4.21	4.15	4.18	4.06
$1^1\Pi_g$	$1\pi_u^{-1}1\delta_u^1$	3.36	3.88	3.83	4.12
$2^1\Delta_g$	$1\pi_u^{-1}1\varphi_u^1$	2.92	3.61	3.54	4.30
$1^1\Pi_u$	$1\pi_u^{-1}1\delta_g^1$	4.33	4.33	4.34	4.17
$2^3\Phi_u$	$2\sigma_g^{-1}1\varphi_u^1$	1.85	2.88	2.76	4.61
$2^1\Phi_u$	$2\sigma_g^{-1}1\varphi_u^1$	1.95	2.97	2.86	4.68
$2^3\Delta_u$	$2\sigma_g^{-1}1\delta_u^1$	2.66	3.49	3.42	4.70
$2^1\Delta_u$	$2\sigma_g^{-1}1\delta_u^1$	2.66	3.45	3.39	4.70
$3^1\Delta_u$	$1\pi_g^{-1}1\varphi_u^1$	3.06	4.04	3.94	5.27
$3^3\Phi_u$	$1\pi_g^{-1}1\delta_u^1$	3.71	4.47	4.40	5.31
$2^3\Pi_u$	$1\pi_g^{-1}1\delta_u^1$	3.71	4.46	4.40	5.35
$3^3\Delta_u$	$1\pi_g^{-1}1\varphi_u^1$	2.95	3.96	3.86	5.36
$1^3\Gamma_u$	$1\pi_g^{-1}1\varphi_u^1$	3.00	3.96	3.86	5.37
$1^1\Gamma_u$	$1\pi_g^{-1}1\varphi_u^1$	2.99	3.94	3.84	5.38
$2^1\Pi_u$	$1\pi_g^{-1}1\delta_u^1$	4.08	4.82	4.74	5.62
$3^1\Phi_u$	$1\pi_g^{-1}1\delta_u^1$	3.76	4.57	4.34	5.86

values of most states being too small by 0.5–2.5 eV. The U.5f type orbitals are rather contracted in comparison to other valence orbitals, though less so than for the lanthanides or the later actinides; they are distributed mainly inside the atomic core and overlap only slightly with the neighboring atoms. Other authors had also found unsatisfactory TDDFT excitation energies for various kinds of uranyl complexes and concluded that most density functionals do not yield accurate excitation energies [21, 23–25]. The asymptotically corrected SAOP potential is indeed somewhat better than the PW91 potential, with errors 'only' up to 1.5 eV, but the small U.5fδ_u/ϕ_u separation is still incorrectly reproduced. A much larger QZ4P basis set brings little improvement, indicating that the TZ2P basis sets used are adequate. Furthermore, our results with the SAOP functional on UN_2 do not reproduce somewhat more reasonable TDDFT trends for UO_2^{2+} found by some other authors [21, 24] as well as in this work. Concerning UN_2, only the lowest four TDDFT energies are in a satisfactory agreement with CASPT2, while the TDDFT/SAOP and CASPT2 energies of all excitations to U.5f are much closer for UO_2^{2+} (Table 3). Moreover, we find the singlet–triplet splitting of the lowest excited $1^{1,3}\Delta_g$ ($2\sigma_u^{-1}1\delta_u^1$) states from TDDFT around 0.55 eV, which is much smaller that the CASPT2 value of 1.04 eV. In contrast, the respective results for UO_2^{2+} are somewhat less deviating, 0.77 and 1.11 eV.

Table 13 NUO^+: Vertical excitation energies (in eV) at the SR level from TDDFT using the PW91 or SAOP functionals and a TZ2P basis set, and from CASPT2

SR state	Leading configuration	TDDFT PW91	TDDFT SAOP	CAS-PT2
$1^3\Delta$	$4\sigma^{-1}1\delta^1$	1.40	2.28	2.40
$1^3\Phi$	$4\sigma^{-1}1\phi_u^1$	0.75	1.89	2.52
$1^1\Phi$	$4\sigma^{-1}1\phi^1$	1.05	2.18	2.86
$1^1\Delta$	$4\sigma^{-1}1\delta^1$	1.78	2.70	3.19
$1^3\Gamma$	$2\pi^{-1}1\phi^1$	1.93	2.89	3.47
$2^3\Delta$	$2\pi^{-1}1\phi^1$	1.94	2.89	3.47
$2^3\Phi$	$2\pi^{-1}1\delta^1$	2.64	3.37	3.54
$1^3\Pi$	$2\pi^{-1}1\delta^1$	2.64	3.37	3.54
$1^1\Gamma$	$2\pi^{-1}1\phi^1$	2.07	3.02	3.57
$2^1\Phi$	$2\pi^{-1}1\delta^1$	2.35	3.29	3.59
$2^1\Delta$	$2\pi^{-1}1\phi^1$	2.68	3.41	3.73
$1^1\Pi$	$2\pi^{-1}1\delta^1$	3.03	3.71	3.81
$3^3\Phi$	$3\sigma^{-1}1\phi^1$	2.97	4.10	5.82
$3^1\Phi$	$3\sigma^{-1}1\phi^1$	3.19	4.31	5.93
$3^3\Delta$	$3\sigma^{-1}1\delta^1$	3.62	4.54	5.91
$3^1\Delta$	$3\sigma^{-1}1\delta^1$	4.03	4.89	6.11
$4^1\Phi$	$1\pi^{-1}1\delta^1$	4.85	5.75	6.58
$4^3\Phi$	$1\pi^{-1}1\delta^1$	4.86	5.71	6.58
$2^3\Pi$	$1\pi^{-1}1\delta^1$		5.71	6.59
$2^3\Gamma$	$1\pi^{-1}1\phi^1$	4.19	5.26	6.70
$2^1\Gamma$	$1\pi^{-1}1\phi^1$	4.24	5.30	6.70
$4^3\Delta$	$1\pi^{-1}1\phi^1$	4.19	5.26	6.72
$4^1\Delta$	$1\pi^{-1}1\phi^1$	4.46	5.44	6.73

A similar comparison for NUO^+ is presented in Table 13. Again, the PW91 and even the SAOP functionals underestimate the most characteristic valence → U.5f excitations, by about 0.5 eV for the lower-lying states and by more than 1 eV for the higher-lying states, both for U–N and for U–O bond excitations.

The calculation results with SO coupling for UN_2 are displayed in Table 14. The trends of the SO energy shifts at the RAS-SI/SO level are qualitatively reproduced at the ZORA-TDDFT level, though not numerically accurate. The order of the total SO-coupled vertical excitation energies from DFT is perturbed in the same manner as mentioned earlier for the SR energies. That is, there are relatively large negative DFT energy errors of various sizes for excitations to U-5f orbitals, but slightly better results for excitations to U-6d and U-7s orbitals. The small radial extension of the U-5f type orbitals suggests that further investigation of the self-interaction error is necessary.

5 Conclusions

The comparison of the excited states of the isoelectronic species $|N\equiv U\equiv N|$, $|N\equiv U\equiv O|^+$ and $|O\equiv U\equiv O|^{2+}$ reveals interesting differences. First, the upper bonding MOs of UN_2 form a nearly equidistant energy ladder, while those of UO_2^{2+} are not only lower but also unevenly distributed, with the $2\sigma_u$ HOMO well separated from the $1\pi_u$ HOMO-1

Table 14 UN_2: SO-coupled vertical excitation energies E and SO contributions $\delta_{SO}E$ (in eV) from ZORA-TDDFT-SAOP and RECP-RAS-SI/SO-PT2 calculations; principal SR state admixtures in % from DFT and RAS

SO state	Principal SR state	E		$\delta_{SO}E$		% of principal SR state	
		TDDFT	RASPT2	TDDFT	RASPT2	TDDFT	RASPT2
$1\Delta_g$	$1^3\Phi_g$	1.62	1.89	−0.4	−0.47	79	89
$1\Phi_g$	$1^3\Phi_g$	1.76	2.03	−0.26	−0.33	55	64
$1\Pi_g$	$1^3\Delta_g$	2.25	2.10	−0.23	−0.22	97	98
$2\Delta_g$	$1^3\Delta_g$	2.43	2.36	−0.05	+0.04	77	80
$2\Phi_g$	$1^3\Delta_g$	2.89	2.73	+0.41	+0.41	72	81
$1\Gamma_g$	$1^3\Phi_g$	2.34	2.75	+0.32	+0.39	98	99
$3\Phi_g$	$1^1\Phi_g$	2.56	3.07	+0.11	+0.21	69	53
$2\Pi_g$	$2^3\Delta_g$	2.58	3.27	−0.41	−0.55	90	98
$2\Gamma_g$	$1^3\Gamma_g$	2.66	3.29	−0.33	−0.53	50	55
$3\Delta_g$	$1^1\Delta_g$	3.21	3.37	+0.18	−0.09	67	47
$1\Sigma_u^-$	$a^3\Sigma_u^+$	2.47	2.48	+0.11	+0.00	95	91
$1\Pi_u$	$a^3\Sigma_u^+$	2.48	2.48	+0.12	+0.00	95	94
$1\Sigma_u^+$	$a^1\Sigma_u^+$	2.70	2.67	−0.16	−0.02	92	90
$2\Pi_u$	$1^3\Delta_u$	2.85	2.75	−0.36	−0.28	95	93
$1\Delta_u$	$1^3\Delta_u$	2.92	2.82	−0.29	−0.21	66	65
$1\Phi_u$	$1^3\Delta_u$	3.28	3.16	+0.07	+0.13	95	82
$2\Delta_u$	$1^1\Delta_u$	3.39	3.26	−0.01	+0.04	62	51
$3\Delta_u$	$a^3\Pi_u$	3.41	3.49	−0.11	+0.08	91	68
$3\Pi_u$	$a^3\Pi_u$	3.52	3.50	+0.00	+0.09	67	68
$2\Phi_u$	$1^3\Phi_u$	3.77	3.72	−0.38	−0.3	99	99

that is near-degenerate with the $2\sigma_g$ HOMO-2 (Fig. 1). Interestingly, NUO^+ is not intermediate, but has two upper N–U bonding MOs like UN_2 and two lower U–O bonding MOs like UO_2^{2+}; in the NUO^+ molecule, however, both pairs of MOs are localized on N–U and U–O, respectively. As a result, larger bond length expansions occur for just one of the two bonds of NUO^+ upon electronic excitation, when compared to the smaller bond length expansions of both bonds of UN_2 or UO_2^{2+}. Accordingly, also much longer vibrational progressions upon UV–Vis absorption or emission are expected for NUO^+.

Second, the pattern of the lower virtual orbitals is different for each of the three species. For UN_2, the non-bonding U.5fϕ_u,fδ_u, U.7sσ_g, and U.6dδ_g are near-degenerate, giving rise to a quite dense set of low-lying excited states. Absorption will occur in most of the visible region, with intense symmetry-allowed excitations to U.7s,6d beginning in the green region. For UO_2^{2+}, the U.5fϕ_u,fδ_u levels are well separated from U.7sσ_g and U.6dδ_g by a large gap of about 3 eV. Excitations to the latter are expected in the far-UV and have so far not been detected. For NUO^+, the virtual level pattern is similar to that of UO_2^{2+}. However, the onset of absorption does not occur in the red, but already in the infrared.

Concerning methodological aspects, a judiciously chosen RASPT2 approach seems sufficient for a reasonable prediction of the spectral properties of actinide compounds. SO-TDDFT approaches with the SAOP functional may predict geometries and spin–orbit splittings of electronically excited states at a qualitatively correct level. However, the energies of excitations into the U.5fϕ,fδ levels from DFT approaches are still unsatisfactory. Further improvements of the exchange–correlation functionals are required to treat excited states of actinide compounds with diverse valence shells. Compared with the difficulty in accurately recovering the electron correlation effects, the important SR and SO relativistic effects are more easily reproducible.

Acknowledgments This work was supported by NKBRSF (2011CB932400) and NSFC (20933003, 11079006, 91026003) of China. The calculations were performed by using supercomputers at the Computer Network Information Center, Chinese Academy of Sciences, Tsinghua National Laboratory for Information Science and Technology, and the Shanghai Supercomputing Center.

References

1. Heinemann C, Marçalo J, de Matos AP, Schwarz H (1996) Angew Chem Int Ed Engl 35:891
2. Gibson JK, Marçalo J (2006) Coord Chem Rev 250:776
3. Groenewold GS, Gianotto AK, Cossel KC, Van Stipdonk MJ, Moore DT, Polfer N, Oomens J, de Jong WA, Visscher L (2006) J Am Chem Soc 128:4802
4. Heinemann C, Schwarz H (1995) Chem Eur J 1:7
5. Zhou M, Andrews L (1999) J Chem Phys 111:11044
6. Hunt RD, Yustein JT, Andrews L (1993) J Chem Phys 98:6070
7. Green DW, Reedy GT (1976) J Chem Phys 65:2921
8. Hunt RD, Andrews L (1993) J Chem Phys 98:3690
9. Kushto GP, Souter PF, Andrews L (1997) J Chem Phys 106:5894
10. Silva GWC, Yeamans CB, Ma L, Cerefice GS, Czerwinski KR, Satteberger AP (2008) Chem Mater 20:3076
11. Lyon JT, Hu HS, Andrews L, Li J (2007) Proc Natl Acad Sci USA 104:18919
12. Li J, Hu HS, Lyon JT, Andrews L (2007) Angew Chem Int Ed 46:9045
13. Hayton TW (2010) Dalton Trans 39:1129
14. Fortier S, Wu GA, Hayton TW (2010) J Am Chem Soc 132:6888
15. Pyykkö P, Li J, Runeberg N (1994) J Phys Chem 98:4809
16. Kaltsoyannis N (2000) Inorg Chem 39:6009
17. Gagliardi L, Roos BO (2000) Chem Phys Lett 331:229
18. Bursten BE, Drummond ML, Li J (2003) Farady Discuss 124:1
19. Moskaleva LV, Matveev AV, Krueger S, Rösch N (2006) Chem Eur J 12:629
20. Pierloot K, van Besien E (2005) J Chem Phys 123:204309
21. Pierloot K, van Besien E, van Lenthe E, Baerends EJ (2007) J Chem Phys 126:194311
22. Pierloot K (2003) Mol Phys 101:2083
23. Réal F, Gomes ASP, Visscher L, Vallet V, Eliav E (2009) J Phys Chem A 113:12504
24. Réal F, Vallet V, Marian C, Wahlgren U (2007) J Chem Phys 127:214302
25. Bast R, Jensen HJA, Saue T (2009) Int J Quantum Chem 109:2091
26. Pepper M, Bursten BE (1991) Chem Rev 91:719
27. Denning RG (2007) J Phys Chem A 111:4125
28. Straka M, Dyall KG, Pyykkö P (2001) Theor Chem Acc 106:393
29. Straka M, Patzschke M, Pyykkö P (2003) Theor Chem Acc 109:332
30. Gagliardi L, Pyykkö P (2004) Angew Chem Int Ed 43:1573
31. Odoh SO, Schreckenbach G (2010) J Phys Chem A 114:1957
32. Olsen J, Roos BO, Jørgensen P, Jensen HJA (1988) J Chem Phys 89:2185
33. MOLPRO, version 2008.1, http://www.molpro.net. Extended reference see SI-file
34. Küchle W, Dolg M, Stoll H, Preuss H (1994) J Chem Phys 100:7535
35. Dunning TH (1989) J Chem Phys 90:1007
36. Malmqvist PÅ, Roos BO, Schimmelpfennig B (2002) Chem Phys Lett 357:230
37. te Velde G, Bickelhaupt FM, van Gisbergen SJA, Fonseca Guerra C, Baerends EJ, Snijders JG, Ziegler T (2001) J Comput Chem 22:931
38. Fonseca Guerra C, Snijders JG, te Velde G, Baerends EJ (1998) Theor Chem Acc 99:391
39. ADF2009.01, SCM, Theoretical Chemistry, Vrije Universiteit, Amsterdam, The Netherlands, http://www.scm.com. Extended reference see SI-file
40. Chang C, Pelissier M, Durand M (1986) Phys Scripta 34:294
41. Faas S, Snijders JG, van Lenthe JH, van Lenthe E, Baerends EJ (1995) Chem Phys Lett 246:632
42. Perdew JP, Chevary JA, Vosko SH, Jackson KA, Pederson MR, Singh DJ, Fiolhais C (1992) Phys Rev B 46:6671
43. Gritsenko OV, Schipper PRT, Baerends EJ (1999) Chem Phys Lett 302:199
44. Schipper PRT, Gritsenko OV, van Gisbergen SJA, Baerends EJ (2000) J Chem Phys 112:1344
45. Van Lenthe E, Baerends EJ (2003) J Comp Chem 24:1142
46. Pyykkö P, Riedel S, Patzscheka M (2005) Chem Eur J 11:3511
47. Meister J, Schwarz WHE (1994) J Phys Chem 98:8245

48. Li J, Bursten BE, Andrews L, Marsden CJ (2004) J Am Chem Soc 126:3424
49. Li J, Bursten BE, Liang B, Andrews L (2002) Science 295:2242
50. Mulliken RS (1972) Chem Phys Lett 14:142
51. Lee HY, Wang SP, Chang TC (2001) Int J Quantum Chem 81:53
52. Burns CJ, Bursten BE (1989) Comments Inorg Chem 9:61